mathematics

MDPI

Article

Relaxed Local Tracking Conditions for Markovian Jump Systems with Application to DC-DC Synchronous Buck Converters Under Load Resistance Switching Variations

Yu Jin Choi and Sung Hyun Kim *

Department of Electrical, Electronic and Computer Engineering, University of Ulsan, Ulsan 44610, Republic of Korea; dbwks1010@naver.com
* Correspondence: shnkim@ulsan.ac.kr

Abstract

This paper presents a local tracking control approach for DC–DC synchronous buck converters operating under randomly varying load resistance. The load variation is represented by a discrete-mode switching mechanism governed by a Markov stochastic process, allowing the converter dynamics to be modeled as a Markovian jump system. A mode-dependent state-feedback controller is developed based on linear matrix inequality (LMI)-based conditions that explicitly incorporate transition-rate information. By incorporating the transition characteristics into the controller design, the proposed method ensures stochastic local stability together with satisfactory tracking performance within a prescribed local stability region, while reducing the conservatism of conventional global-stability-based approaches. Simulation studies demonstrate that the proposed controller effectively regulates the converter under stochastic load variations.

Keywords: DC-DC buck converter; Markovian jump systems; local stabilization; transition-rate-dependent

MSC: 93C95; 93E15

1. Introduction

A DC–DC buck converter is one of the most widely adopted power converters for supplying a regulated low-voltage output from a higher input voltage owing to its simple structure and high conversion efficiency [1–4]. In practical applications such as smartphones, IoT devices, and LED lighting systems, abrupt changes in operating conditions frequently cause the load resistance to vary unpredictably, resulting in significant degradation of voltage regulation and transient performance. Conventional converter models generally assume constant or piecewise-constant loads [5], which are often insufficient to describe these stochastic operating conditions. To provide a more realistic representation, this paper models randomly varying load conditions as a Markovian jump system (MJS), where the converter switches probabilistically among multiple operating modes according to predefined transition rates [6–8]. An MJS consists of a finite number of modes governed by a Markov stochastic process [9,10], and each mode is associated with different system dynamics whose switching behavior is characterized by transition rates [11,12]. Consequently, the MJS framework naturally captures random structural changes and parameter variations from a probabilistic viewpoint, providing an effective control-oriented model for practical systems subject to stochastic operating conditions [13,14]. Furthermore, incorporating

Check for updates

Academic Editor: Alma Y. Alanis

Received: 25 June 2026
Revised: 15 July 2026
Accepted: 30 July 2026
Published: 2 August 2026

Copyright: © 2026 by the authors. Licensee MDPI, Basel, Switzerland. This article is an open access article distributed under the terms and conditions of the Creative Commons Attribution (CC BY) license.

transition-rate information into the controller design allows the statistical characteristics of load-mode transitions to be explicitly considered, rather than treating them simply as unknown disturbances.

Recently, considerable attention has been devoted to control design for Markovian jump systems, particularly local stabilization methods that guarantee stability only inside a prescribed domain of attraction [15,16]. Existing studies mainly construct ellipsoidal attraction regions using mode-dependent Lyapunov functions and exploit transition-rate information to reduce the conservatism of stabilization conditions [17,18]. Nevertheless, transition-rate uncertainties are still frequently treated conservatively, leading to unnecessarily restrictive LMI conditions [19,20]. Meanwhile, most tracking controllers for DC–DC converters are developed within a global stabilization framework, where stability is required over the entire admissible state space. Some methods additionally employ actuator or duty-ratio saturation to indirectly limit the state trajectories. Although these approaches provide satisfactory regulation performance under normal operating conditions, they neither explicitly define the admissible tracking region nor fully utilize stochastic mode-transition information during controller synthesis. Consequently, existing studies largely focus on regulation rather than tracking, and a unified framework capable of simultaneously addressing local stochastic stability and tracking performance has remained largely unexplored [21].

Motivated by the above observations, this paper proposes a transition-rate-dependent local stochastic tracking control framework for DC–DC synchronous buck converters with randomly varying load resistance. The main contributions of this paper are summarized as follows.

- A transition-rate-dependent stochastic tracking controller is developed for Markovian jump buck converters. Unlike conventional global tracking controllers, the proposed method explicitly incorporates transition-rate information into the LMI synthesis, which enables the controller to account for stochastic load-mode transitions while reducing the conservatism of existing global-stability-based approaches [22].
- A local stochastic tracking framework is established by introducing a predefined domain of attraction. In contrast to existing methods that guarantee tracking over the entire admissible state space or indirectly restrict state excursions through input saturation, the proposed approach explicitly specifies the admissible operating region. This leads to improved transient responses while effectively suppressing excessive inductor-current peaks, thereby enhancing the protection of power electronic components under practical duty-ratio constraints [23].
- The effectiveness of the proposed controller is verified through simulations under various Markovian jump load scenarios. The results demonstrate faster transient responses, improved tracking accuracy, enhanced robustness, and less conservative performance compared with existing LMI-based tracking methods.

Notations: The following notations will be utilized in the main discussion: $X \geq 0$ ($X > 0$) denotes that the matrix X is positive semi-definite (or positive definite, respectively). $(*)$ represents the symmetric term in a matrix expression, indicating that the corresponding symmetric components are included implicitly. $\mathbf{diag}(\cdot)$ denotes the block-diagonal matrix constructed by placing the given matrices along the diagonal. $\left[\mathcal{Q}_i\right]_{i\in\{1,2,\cdots,s\}} = \begin{bmatrix} \mathcal{Q}_1^T & \mathcal{Q}_2^T & \cdots & \mathcal{Q}_s^T \end{bmatrix}^T$, and $\left[\mathcal{Q}_i\right]^{\mathbf{d}}_{i\in\{1,2,\cdots,s\}} = \mathbf{diag}(\mathcal{Q}_1, \mathcal{Q}_2, \cdots, \mathcal{Q}_s)$.

2. System Modeling

On a given complete probability space, let us consider the process $\{\phi(t) \in \mathbb{N}_s = \{1, \cdots, s\},\ t \geq 0\}$, described as a nonhomogeneous Markov process with the following transition probabilities (TPs) [24]:

$$\mathbf{Pr}(\phi(t+\delta) = h \mid \phi(t) = g) = \begin{cases} \theta_{gh}(t)\delta + o(\delta) & \text{if } h \neq g \\ 1 + \theta_{gg}(t)\delta + o(\delta) & \text{if } h = g \end{cases}$$

where $o(\delta)$ denotes the little-o notation, defined by $\lim_{\delta \to 0}(o(\delta)/\delta) = 0$, and $\theta_{gh}(t)$ indicates the transition rate (TR) from mode g to mode h at time $t + \delta t$, satisfying

$$0 \leq \theta_{gh}(t) \in \left[\underline{\theta}_{gh}, \overline{\theta}_{gh}\right],\ \forall h \in \mathbb{N}_s \backslash \{g\} \tag{1}$$

$$0 = \sum_{h \in \mathbb{N}_\phi} \theta_{gh}(t) \left(\text{i.e., } \theta_{gg}(t) = -\sum_{h \in \mathbb{N}_s \backslash \{g\}} \theta_{gh}(t) \in \left[\underline{\theta}_{gg}, \overline{\theta}_{gg}\right] \right). \tag{2}$$

Based on (1) and (2), the transition rate can be described as follows:

$$\theta_{gh}(t) = \rho_{gh} + \delta_{gh}(t) \text{ subject to } \delta_{gh}(t) \in \left[-\bar{\delta}_{gh}, \bar{\delta}_{gh}\right] \tag{3}$$

where

$$\rho_{gh} = \frac{\underline{\theta}_{gh} + \overline{\theta}_{gh}}{2},\ \bar{\delta}_{gh} = \frac{\overline{\theta}_{gh} - \underline{\theta}_{gh}}{2}.$$

In what follows, let us consider the circuit of the DC-DC synchronous buck converter (see Figure 1), where $R_g = R(\phi(t) = g)$ denotes a piecewise constant load resistance that changes stepwise according to the load-side operating mode $\phi(t) \in \mathbb{N}_s$ (e.g., LEDs being switched on or off). Then, when Q1 is turned on and Q2 is turned off, the time derivative of the inductor current can be expressed as follows:

$$\begin{aligned} \dot{i}_L(t) &= -\frac{1}{L}v_O(t) - \frac{1}{L}(R_{DS} + R_{DCR})i_L(t) + \frac{1}{L}v_I(t) \\ &= -\frac{1}{L}\left(\frac{R_g R_{ESR}}{R_g + R_{ESR}} + R_{DS} + R_{DCR}\right)i_L(t) - \frac{1}{L}\frac{R_g}{R_g + R_{ESR}}v_C(t) + \frac{v_I(t)}{L} \end{aligned} \tag{4}$$

where $i_L(t)$ and $v_C(t)$ represent the inductor current and the capacitor voltage of the converter, respectively; $v_I(t)$ denotes the input voltage of the power source; L denotes the inductance determined by the design specifications; R_{DCR} and R_{ESR} represent the equivalent series resistance of the inductor and capacitor, respectively; and R_{DS} represents the static drain-to-source resistance of the high-side and low-side power MOSFETs. In the opposite case, it is given as follows:

$$\begin{aligned} \dot{i}_L(t) &= -\frac{1}{L}v_O(t) - \frac{1}{L}(R_{DS} + R_{DCR})i_L(t) \\ &= -\frac{1}{L}\left(\frac{R_g R_{ESR}}{R_g + R_{ESR}} + R_{DS} + R_{DCR}\right)i_L(t) - \frac{1}{L}\frac{R_g}{R_g + R_{ESR}}v_C(t). \end{aligned} \tag{5}$$

Then, based on the averaging method for one-time-scale discontinuous systems [25], the combination of (4) and (5) leads to the following inductor current dynamics:

$$\dot{i}_L(t) = -\frac{1}{L}v_O(t) - \frac{1}{L}(R_{DS} + R_{DCR})i_L(t) + \frac{1}{L}e(t)$$
$$= -\kappa_{1g}i_L(t) - \kappa_{2g}v_C(t) + \kappa_3 e(t) \quad (6)$$
$$e(t) = v_I(t)d(t) \quad (7)$$

where $d(t)$ denotes the duty ratio of the PWM buck converter, and

$$\kappa_{1g} = \frac{1}{L}\left(\frac{R_g R_{ESR}}{R_g + R_{ESR}} + R_{DS} + R_{DCR}\right),$$
$$\kappa_{2g} = \frac{1}{L}\frac{R_g}{R_g + R_{ESR}},\ \kappa_3 = \frac{1}{L}.$$

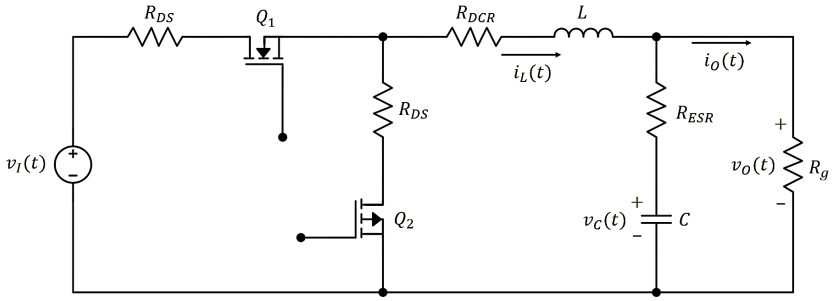


Figure 1. Equivalent circuit of the synchronous buck converter .

In addition, the capacitor voltage dynamics are given by

$$\dot{v}_C(t) = \kappa_{4g}i_L(t) - \kappa_{5g}v_C(t) \quad (8)$$

where

$$\kappa_{4g} = \frac{1}{C}\frac{R_g}{R_g + R_{ESR}},\ \kappa_{5g} = \frac{1}{C}\frac{1}{R_g + R_{ESR}}$$

in which C denotes the capacitance determined by the given design specifications. As is well known, the control objective of the DC–DC buck converter is to regulate $v_O(t)$ to a prescribed constant level, denoted by $\bar{v}_O$, under the mode-dependent constant resistance R_g. In other words, since $\dot{v}_C(t) = (v_O(t) - v_C(t))/(CR_{ESR})$, it is required that the steady-state value of $v_C(t)$ becomes $\bar{v}_C = \bar{v}_O$. Simultaneously, based on (6) and (8), the steady-state values of $i_L(t)$ and $e(t)$ satisfy the following relations, respectively:

$$0 = -\kappa_{1g}\bar{i}_{L,g} - \kappa_{2g}\bar{v}_C + \kappa_3\bar{e}_g \quad (9)$$
$$0 = \kappa_{4g}\bar{i}_{L,g} - \kappa_{5g}\bar{v}_C \quad (10)$$

which leads to

$$\bar{e}_g = \left(\frac{R_g R_{ESR}}{R_g + R_{ESR}} + R_{DS} + R_{DCR}\right)\bar{i}_{L,g} + \frac{R_g}{R_g + R_{ESR}}\bar{v}_C \quad (11)$$
$$\bar{v}_C = R_g\bar{i}_{L,g}. \quad (12)$$

Combining (11) and (12) yields

$$\begin{aligned}\bar{e}_g &= \left(\frac{R_g R_{ESR}}{R_g+R_{ESR}}+R_{DS}+R_{DCR}\right)\frac{\bar{v}_C}{R_g}+\frac{R_g}{R_g+R_{ESR}}\bar{v}_C \\ &= \left(1+\frac{R_{DS}+R_{DCR}}{R_g}\right)\bar{v}_C. \end{aligned} \tag{13}$$

By defining $x_1(t) = i_L(t) - \bar{i}_{L,g}$, $x_2(t) = v_C(t) - \bar{v}_C$, and $u(t) = e(t) - \bar{e}_g$, the error state dynamics are formulated from (6) and (8) as follows:

$$\begin{aligned}\dot{x}_1(t) &= -\kappa_{1g}x_1(t) - \kappa_{2g}x_2(t) + \kappa_3 u(t) + \big(-\kappa_{1g}\bar{i}_{L,g} - \kappa_{2g}\bar{v}_C + \kappa_3\bar{e}_g\big) \\ \dot{x}_2(t) &= \kappa_{4g}x_1(t) - \kappa_{5g}x_2(t) + \big(\kappa_{4g}\bar{i}_{L,g} - \kappa_{5g}\bar{v}_C\big).\end{aligned}$$

Accordingly, it follows from (9) and (10) that

$$\dot{x}(t) = A_g x(t) + Bu(t) \tag{14}$$

where $x(t) = \mathbf{col}(x_1(t), x_2(t)) \in \mathbb{R}^n$, $u(t) \in \mathbb{R}^m$, and

$$A_g = \begin{bmatrix} -\kappa_{1g} & -\kappa_{2g} \\ \kappa_{4g} & -\kappa_{5g} \end{bmatrix},\ B = \begin{bmatrix} \kappa_3 \\ 0 \end{bmatrix}.$$

For the error-state system (14), this paper aims to develop the following mode-dependent state-feedback control law:

$$u(t) = K_g x(t) \tag{15}$$

where K_g is the mode-dependent control gain to be designed.

Remark 1. *The proposed mode-dependent state-feedback controller is particularly suitable for Markovian jump systems because it explicitly exploits both the current operating mode and the associated transition-rate information. This enables the controller to respond systematically to stochastic mode switching, which results in less conservative stabilization conditions and improved transient performance.*

Thus, the closed-loop system is described as follows:

$$\dot{x}(t) = \big(A_g + BK_g\big)x(t) \tag{16}$$

where the control gain K_g will be designed such that the error state $x(t)$ is subject to

$$x(t) \in \mathcal{L}(\bar{x}) := \Big\{x \in \mathbb{R}^n \mid |\mathbf{e}_\iota^T x| \le \bar{x}_\iota,\ \iota \in \mathbb{N}_n\Big\}$$

where $\bar{x}_\iota$ is a given positive constant, and $\mathbf{e}_\iota$ is a unit vector with the ιth nonzero entry, i.e., $\mathbf{e}_1 = \mathbf{col}(1,0)$ and $\mathbf{e}_2 = \mathbf{col}(0,1)$.

The following definitions will play a key role in designing a stochastically local tracking controller based on the given TR information.

Definition 1. *For the initial state $x(0)$ and the initial mode $\phi(0)$, the closed-loop system (16) is stochastically stable if the following condition holds:*

$$\lim_{T\to\infty} \mathbf{E}\left\{\int_0^T \|x(t)\|^2 dt \mid x(0), \phi(0)\right\} < \infty \tag{17}$$

Definition 2. *For any initial condition $x(0)$ and $\phi(0)$, suppose that it holds that*

$$\lim_{t\to\infty} \mathbf{E}\left\{ \int_0^t \|x(\tau)\|^2 d\tau \mid x(0), \phi(0) \right\} < \infty \tag{18}$$

$$x(t) \in \mathcal{L}(\bar{x}) \tag{19}$$

$$x(0) \in \mathcal{L}_0 \subset \mathcal{L}(\bar{x}). \tag{20}$$

Then, $\mathcal{L}_0$ becomes the domain of attraction, and closed-loop system (14) is locally stochastically stable in $\mathcal{L}(\bar{x})$.

Remark 2. *The Markovian jump model provides a practical and well-established framework for describing randomly switching load conditions in buck converters. Since practical operating conditions typically evolve among a finite number of discrete load modes, a finite-state Markov process offers an effective representation of the load dynamics and has been widely adopted in the modeling and control of stochastic power electronic systems.*

Remark 3. *The operating modes considered in this paper represent representative load-resistance levels corresponding to typical operating conditions of practical buck converters. Such a finite-state approximation is widely adopted in Markovian jump system modeling to represent continuous load variations, and the proposed control framework can be readily extended to accommodate a larger number of operating modes when a finer approximation is desired.*

Remark 4. *The proposed control framework assumes that the Markov transition-rate matrix is available. In practical applications, the transition rates can be identified or estimated from measured load-switching data using statistical or system-identification techniques (see [26]).*

3. Stabilization Conditions

The following mode-dependent Lyapunov function is selected [27]:

$$V(t) = x^T(t) P(\phi(t)) x(t) \tag{21}$$

where $0 < P(\phi(t) = g) = P_g = P_g^T \in \mathbb{R}^{n_x}$. Accordingly, applying the weak infinitesimal operator to $V(t, \phi(t))$ yields

$$\begin{aligned}
\nabla V(t) &= \lim_{\delta\to 0} \frac{1}{\delta} \mathbf{E}\Big\{ V(t+\delta, \phi(t+\delta) = h \mid \phi(t) = g) - V(t,g) \Big\} \\
&= \lim_{\delta\to 0} \frac{1}{\delta} \Bigg(\sum_{h\in\mathbb{N}_s\setminus\{g\}} \Big(\theta_{gh}(t)\delta + o(\delta)\Big) V(t+\delta, h) \\
&\qquad + \Big(1 + \theta_{gg}(t)\delta + o(\delta)\Big) V(t+\delta, g) - V(t,g) \Bigg) \\
&= \sum_{h\in\mathbb{N}_s} \theta_{gh}(t) V(t,h) + \dot{V}(t,g).
\end{aligned} \tag{22}$$

The following lemma presents the local stabilization conditions for (16), where the domain of attraction (DOA) is characterized as $\mathcal{L}_0 := \mathcal{E}(Q, \beta)$.

Lemma 1. *For a given $\alpha > 0$, suppose that there exist symmetric matrices $0 < P_g$ and $0 < Q \in \mathbb{R}^{n\times n}$, and a positive scalar β, such that the following holds:*

$$0 > \nabla V(t) + \alpha V(t) \tag{23}$$

$$0 < \begin{bmatrix} \beta^{-1} & \mathbf{e}_\iota^T \\ (*) & \bar{x}_\iota^2 P_g \end{bmatrix}, \ \forall \iota \in \mathbb{N}_n, \ g \in \mathbb{N}_s \tag{24}$$

$$0 \geq P_g - Q, \ \forall g \in \mathbb{N}_s \tag{25}$$

Then, the closed-loop system (16) is locally stochastically stable within $\mathcal{L}(\bar{x})$.

Proof. To begin with, let us define the following ellipsoid:

$$\mathcal{L}_g = \mathcal{E}(P_g, \beta).$$

From (25), it follows that $\beta^{-1}P_g \leq \beta^{-1}Q$, which means that $x(0) \in \mathcal{L}_0 \subseteq \mathcal{L}_g$. In addition, $\mathcal{L}_g \subset \mathcal{L}(\bar{x})$ is equivalent to

$$\left(\mathbf{e}_\iota \mathbf{e}_\iota^T\right)\bar{x}_\iota^{-2} < P_g\beta^{-1}$$

whose Schur complement leads to (24). Thus, conditions (24) and (25) ensure that $x(0) \in \mathcal{L}_0 \subseteq \mathcal{L}_g \subset \mathcal{L}(\bar{x})$, i.e., (20) in Definition 2.

Next, note that by the generalized Dynkin's formula, it follows that

$$\mathbf{E}\left\{\int_0^t \nabla V(\tau)d\tau \mid x(0) \in \mathcal{L}_0, \phi(0)\right\} = \mathbf{E}\{V(t)\} - V(0). \tag{26}$$

Thus, condition (23) implies

$$\mathbf{E}\{V(t)\} - V(0) < -\mathbf{E}\left\{\int_0^t \alpha V(\tau)d\tau \mid x(0) \in \mathcal{L}_0, \phi(0)\right\} < 0. \tag{27}$$

Furthermore, owing to the positiveness of $V(t)$, we can choose a sufficiently small positive κ such that $\alpha V(\tau) \geq \kappa\|x(\tau)\|_2^2$, which leads to

$$-V(0) < -\mathbf{E}\left\{\int_0^t \kappa\|x(\tau)\|_2^2 d\tau \mid x(0) \in \mathcal{L}_0, \phi(0)\right\}$$

that is, $\lim_{t\to\infty} \mathbf{E}\left\{\int_0^t \|x(\tau)\|_2^2 d\tau \mid x(0) \in \mathcal{L}_0, \phi(0)\right\} < \kappa^{-1}V(0)$ i.e., (18) in Definition 2.

Finally, by (27), it is given that $\mathbf{E}\{V(t)\} < V(0)$. Furthermore, since (25) ensures that $P(\phi(t)) \leq Q$ for all $t \geq 0$ (as (25) must hold for all g), it follows that $V(0) = x^T(0)P(\phi(0))x(0) \leq x^T(0)Qx(0) \leq \beta$. Thus, it is ensured that $\mathbf{E}\{V(t)\} < \beta$, which indicates that $x(t) \in \mathbf{E}\{\mathcal{E}(P_g, \beta)\}$. Accordingly, from the fact that (24) guarantees that $\mathcal{L}_g = \mathcal{E}(P_g, \tau) \subset \mathcal{L}(\bar{x})$, it holds that $x(t) \in \mathcal{L}(\bar{x})$, i.e., (19) in Definition 2. □

The following lemma provides the local stabilization conditions corresponding to (23)–(25) of Lemma 1, formulated in terms of time-varying transition-rate-dependent linear matrix inequalities.

Lemma 2. *For given $\alpha > 0$ and μ, suppose that there exist matrices $0 < \bar{P}_g = \bar{P}_g^T$, $0 < \bar{Q} = \bar{Q}^T$, $\bar{W} \in \mathbb{R}^{n\times n}$, $\bar{K}_g \in \mathbb{R}^{m\times n}$, and a positive scalar β, such that the following conditions hold:*

$$0 > \begin{bmatrix} \mathbf{He}\{-\bar{W}\} & \bar{P}_g + \mu\bar{W} + A_g\bar{W} + B\bar{K}_g \\ (*) & \mathbf{He}\{-\mu\bar{P}_g\} + \bar{\mathbf{P}}_g + \alpha\bar{P}_g \end{bmatrix} \tag{28}$$

$$0 < \begin{bmatrix} \beta^{-1} & \mathbf{E}_\iota^T\bar{W} \\ (*) & \bar{x}_\iota^2\bar{P}_g \end{bmatrix}, \ \forall \iota \in \mathbb{N}_n, \ g \in \mathbb{N}_s \tag{29}$$

$$0 \geq \bar{P}_g - \bar{Q}, \ \forall g \in \mathbb{N}_s \tag{30}$$

where

$$\bar{\mathbf{P}}_g = \sum_{h\in\mathbb{N}_s} \theta_{gh}(t)\bar{P}_h.$$

Then, the closed-loop system (16) is locally stochastically stable within $\mathcal{L}(\bar{x})$, and the mode-dependent control gain is constructed by $K_g = \bar{K}_g\bar{W}^{-1}$.

Proof. From (21) and (22), it follows that

$$\nabla V(t) + \alpha V(t) = \eta^T(t)\left[\begin{array}{c|c} 0 & P_g \\ \hline P_g & \mathbf{P}_g + \alpha P_g \end{array}\right]\eta(t), \ \eta(t) := \frac{\dot{x}(t)}{x(t)} \tag{31}$$

where

$$\mathbf{P}_g = \sum_{h\in\mathbb{N}_s} {}_{gh}(t)P_h.$$

In addition, based on (16), it holds that

$$0 = 2\eta^T(t)\left[\begin{array}{c|c} W & \mu W \end{array}\right]^T\left[\begin{array}{c|c} -I & A_g + BK_g \end{array}\right]\eta(t) \tag{32}$$

where $W \in \mathbb{R}^{n\times n}$ is a nonsingular matrix. Combining (31) and (32) yields

$$\nabla V(t) + \alpha V(t) = \eta^T(t)\Gamma_g\eta(t) \tag{33}$$

where

$$\Gamma_g := \left[\begin{array}{c|c} 0 & P_g \\ \hline P_g & \mathbf{P}_g + \alpha P_g \end{array}\right] + \mathbf{He}\left\{\left[\begin{array}{c|c} W & \mu W \end{array}\right]^T\left[\begin{array}{c|c} -I & A_g + BK_g \end{array}\right]\right\}.$$

Thus, condition (23) holds if $\Gamma_g < 0$ is satisfied. Furthermore, under a congruent transformation, condition (23) is satisfied if it holds that

$$0 > \left[\begin{array}{c|c} \bar{W} & -\mu\bar{W} \\ \hline 0 & \bar{W} \end{array}\right]^T\Gamma_g\left[\begin{array}{c|c} \bar{W} & -\mu\bar{W} \\ \hline 0 & \bar{W} \end{array}\right] \tag{34}$$

where $\bar{W} := W^{-1}$ is also nonsingular. Accordingly, defining

$$\bar{P}_g := \bar{W}^T P_g\bar{W}, \ \bar{\mathbf{P}}_g := \bar{W}^T\left(\sum_{h\in\mathbb{N}_s}\theta_{gh}(t)P_h\right)\bar{W} = \sum_{h\in\mathbb{N}_s}\theta_{gh}(t)\bar{P}_h, \ \bar{K}_g := K_g\bar{W}$$

condition (34) can be converted into (28).

Next, by pre- and post-multiplying (24) by $\mathbf{diag}(1, \bar{W}^T)$ and its transpose, we can obtain (29). Furthermore, by pre- and post-multiplying (25) by $\bar{W}^T$ and $\bar{W}$, we can derive (30), where $\bar{Q} = \bar{W}^T Q \bar{W}$. □

The following theorem provides the local stabilization conditions corresponding to (28)–(30), formulated in terms of linear matrix inequalities (LMIs).

Theorem 1. *For given $\alpha > 0$ and μ, suppose that there exist matrices $0 < \bar{P}_g = \bar{P}_g^T$, $0 < \bar{Q} = \bar{Q}^T$, $\bar{W} \in \mathbb{R}^{n\times n}$, $\bar{K}_g \in \mathbb{R}^{m\times n}$, $X_{gh} = X_{gh}^T \in \mathbb{R}^{n\times n}$, and a positive scalar $\bar{\beta} = \beta^{-1}$, such that the following conditions hold:*

$$0 > \left[\begin{array}{cc|c} \mathbf{He}\{-\bar{W}\} & \bar{P}_g+\mu\bar{W}+A_g\bar{W}+B\bar{K}_g & 0 \\ (*) & (2,2) & (*) \\ \hline 0 & \left[\frac{1}{2}(\bar{P}_h-\bar{P}_g)\right]_{h\in\mathbb{N}_s\setminus\{g\}} & \left[X_{gh}\right]^{\mathbf{d}}_{h\in\mathbb{N}_s\setminus\{g\}} \end{array}\right] \tag{35}$$

$$0 < \left[\begin{array}{cc} \bar{\beta} & \mathbf{E}_\iota^T\bar{W} \\ (*) & \bar{x}_\iota^2\bar{P}_g \end{array}\right], \ \forall \iota \in \mathbb{N}_n, \ g \in \mathbb{N}_s \tag{36}$$

$$0 \geq \bar{P}_g - \bar{Q}, \ \forall g \in \mathbb{N}_s \tag{37}$$

where

$$(2,2) = -2\mu\bar{P}_g + \alpha\bar{P}_g + \sum_{h\in\mathbb{N}_s\setminus\{g\}} \rho_{gh}(\bar{P}_h - \bar{P}_g) - \sum_{h\in\mathbb{N}_s\setminus\{g\}} \bar{\delta}_{gh}^2 X_{gh}.$$

Then, the closed-loop system (16) is locally stochastically stable within $\mathcal{L}(\bar{x})$, and the mode-dependent control gain is constructed as follows:

$$K_g = \bar{K}_g \bar{W}^{-1}.$$

Proof. From (2) and (3), it follows that

$$\begin{aligned} \bar{\mathbf{P}}_g &= \sum_{h\in\mathbb{N}_s} \theta_{gh}(t)\bar{P}_h = \sum_{h\in\mathbb{N}_s\setminus\{g\}} \theta_{gh}(t)(\bar{P}_h - \bar{P}_g) \\ &= \sum_{h\in\mathbb{N}_s\setminus\{g\}} (\rho_{gh} + \delta_{gh}(t))(\bar{P}_h - \bar{P}_g). \end{aligned}$$

Thus, condition (28) can be described as follows:

$$\begin{aligned} 0 > &\left[\begin{array}{c|c} \mathbf{He}\{-\bar{W}\} & \bar{P}_g + \mu\bar{W} + A_g\bar{W} + B\bar{K}_g \\ \hline (*) & \mathbf{He}\{-\mu\bar{P}_g\} + \alpha\bar{P}_g + \sum_{h\in\mathbb{N}_s\setminus\{g\}} \rho_{gh}(\bar{P}_h - \bar{P}_g) \end{array}\right] \\ &+ \left[\frac{0}{I}\right] \left(\sum_{h\in\mathbb{N}_s\setminus\{g\}} \delta_{gh}(t)(\bar{P}_h - \bar{P}_g) \right) \left[\begin{array}{c|c} 0 & I \end{array}\right]. \end{aligned} \tag{38}$$

Furthermore, by defining $\Delta_g(t) = \left[\delta_{gh}(t)\right]_{h\in\mathbb{N}_s\setminus\{g\}}$, it is obtained that

$$\begin{aligned} &\left[\frac{0}{I}\right] \left(\sum_{h\in\mathbb{N}_s\setminus\{g\}} \delta_{gh}(t)(\bar{P}_h - \bar{P}_g) \right) \left[\begin{array}{c|c} 0 & I \end{array}\right] \\ &= \mathbf{He}\left\{ \left(\Delta_g^T(t) \otimes \left[\frac{0}{I}\right] \right) \left[\begin{array}{c|c} 0 & \frac{1}{2}(\bar{P}_h - \bar{P}_g) \end{array}\right]_{h\in\mathbb{N}_s\setminus\{g\}} \right\} \end{aligned}$$

and thus (38) can be rewritten as follows:

$$0 > \left[\begin{array}{c|c} \mathbf{He}\{-\bar{W}\} & \bar{P}_g + \mu\bar{W} + A_g\bar{W} + B\bar{K}_g \\ \hline (*) & \mathbf{He}\{-\mu\bar{P}_g\} + \alpha\bar{P}_g + \sum\limits_{h\in\mathbb{N}_s\setminus\{g\}} \rho_{gh}(\bar{P}_h - \bar{P}_g) \end{array}\right] + \mathbf{He}\left\{\bar{\Delta}_g^T(t)\left[\begin{array}{c|c} 0 & \frac{1}{2}(\bar{P}_h - \bar{P}_g) \end{array}\right]_{h\in\mathbb{N}_s\setminus\{g\}}\right\} \tag{39}$$

where $\bar{\Delta}_g^T(t) = \Delta_g^T(t) \otimes \left[\begin{array}{cc} 0 & I \end{array}\right]^T$. Using a completion-of-squares argument (equivalently, a quadratic matrix identity), and noting

$$\left[\begin{array}{c|c} 0 & \frac{1}{2}(\bar{P}_h - \bar{P}_g) \end{array}\right]_{h\in\mathbb{N}_s\setminus\{g\}} = \left[\begin{array}{c|c} 0 & \left[\begin{array}{c} \frac{1}{2}(\bar{P}_h - \bar{P}_g) \end{array}\right]_{h\in\mathbb{N}_s\setminus\{g\}} \end{array}\right]$$

condition (39) can be converted into

$$0 > \left[\begin{array}{c} I \\ \hline \bar{\Delta}_g(t) \end{array}\right]^T \mathbf{M}_1 \left[\begin{array}{c} I \\ \hline \bar{\Delta}_g(t) \end{array}\right] \tag{40}$$

where

$$\mathbf{M}_1 = \left[\begin{array}{cc|c} \mathbf{He}\{-\bar{W}\} & \bar{P}_g + \mu\bar{W} + A_g\bar{W} + B\bar{K}_g & 0 \\ (*) & \mathbf{He}\{-\mu\bar{P}_g\} + \alpha\bar{P}_g + \sum\limits_{h\in\mathbb{N}_s\setminus\{g\}} \rho_{gh}(\bar{P}_h - \bar{P}_g) & (*) \\ \hline 0 & \left[\begin{array}{c} \frac{1}{2}(\bar{P}_h - \bar{P}_g) \end{array}\right]_{h\in\mathbb{N}_s\setminus\{g\}} & 0 \end{array}\right].$$

For each $h \in \mathbb{N}_s \setminus \{g\}$, the bounded transition-rate uncertainty $\delta_{gh}(t) \in [-\bar{\delta}_{gh}, \bar{\delta}_{gh}]$ satisfies

$$\left(\delta_{gh}(t) + \bar{\delta}_{gh}\right)\left(\delta_{gh}(t) - \bar{\delta}_{gh}\right) = \delta_{gh}^2(t) - \bar{\delta}_{gh}^2 \leq 0.$$

Moreover, since $X_{gh} = X_{gh}^T < 0$, it follows that

$$\sum_{h\in\mathbb{N}_s\setminus\{g\}} \left(\delta_{gh}^2(t) - \bar{\delta}_{gh}^2\right) \left[\begin{array}{c} 0 \\ I \end{array}\right]^T X_{gh} \left[\begin{array}{c} 0 \\ I \end{array}\right] \geq 0.$$

Accordingly, the boundedness condition on the transition-rate uncertainties can be represented by the quadratic constraint

$$\left[\begin{array}{c} I \\ \hline \bar{\Delta}_g(t) \end{array}\right]^T \mathbf{M}_2 \left[\begin{array}{c} I \\ \hline \bar{\Delta}_g(t) \end{array}\right] \geq 0$$

where

$$\mathbf{M}_2 = \left[\begin{array}{cc|c} 0 & 0 & 0 \\ 0 & -\sum\limits_{h\in\mathbb{N}_s\setminus\{g\}} \bar{\delta}_{gh}^2 X_{gh} & 0 \\ \hline 0 & 0 & \left[\begin{array}{c} X_{gh} \end{array}\right]_{h\in\mathbb{N}_s\setminus\{g\}}^{\mathbf{d}} \end{array}\right].$$

The S-procedure is now employed to remove the explicit dependence on $\bar{\Delta}_g(t)$. In particular, a sufficient condition ensuring $\begin{bmatrix} I \\ \bar{\Delta}_g(t) \end{bmatrix}^T \mathbf{M}_1 \begin{bmatrix} I \\ \bar{\Delta}_g(t) \end{bmatrix} < 0$ for every admissible uncertainty satisfying $\begin{bmatrix} I \\ \bar{\Delta}_g(t) \end{bmatrix}^T \mathbf{M}_2 \begin{bmatrix} I \\ \bar{\Delta}_g(t) \end{bmatrix} \geq 0$ is

$$\mathbf{M}_1 + \mathbf{M}_2 < 0.$$

Indeed, for any admissible $\bar{\Delta}_g(t)$, one has

$$\begin{aligned} &\begin{bmatrix} I \\ \bar{\Delta}_g(t) \end{bmatrix}^T \mathbf{M}_1 \begin{bmatrix} I \\ \bar{\Delta}_g(t) \end{bmatrix} \\ &= \begin{bmatrix} I \\ \bar{\Delta}_g(t) \end{bmatrix}^T (\mathbf{M}_1 + \mathbf{M}_2) \begin{bmatrix} I \\ \bar{\Delta}_g(t) \end{bmatrix} - \begin{bmatrix} I \\ \bar{\Delta}_g(t) \end{bmatrix}^T \mathbf{M}_2 \begin{bmatrix} I \\ \bar{\Delta}_g(t) \end{bmatrix} < 0 \end{aligned}$$

because $\mathbf{M}_1 + \mathbf{M}_2 < 0$ and $\begin{bmatrix} I \\ \bar{\Delta}_g(t) \end{bmatrix}^T \mathbf{M}_2 \begin{bmatrix} I \\ \bar{\Delta}_g(t) \end{bmatrix} \geq 0$. Thus, the uncertainty-dependent inequality (40) is relaxed into the uncertainty-independent LMI $\mathbf{M}_1 + \mathbf{M}_2 < 0$, which is equivalent to (35). Finally, conditions (36) and (37) follow directly from (29) and (30), respectively. □

The following corollary presents the global stabilization conditions for (16), formulated in terms of LMIs.

Corollary 1. *For given $\alpha > 0$ and μ, suppose that there exist matrices $0 < \bar{P}_g = \bar{P}_g^T$, $\bar{W} \in \mathbb{R}^{n\times n}$, $\bar{K}_g \in \mathbb{R}^{m\times n}$, and $X_{gh} = X_{gh}^T \in \mathbb{R}^{n\times n}$, such that the following conditions hold:*

$$0 > \left[\begin{array}{c|cc} \mathbf{He}\{-\bar{W}\} & \bar{P}_g+\mu\bar{W}+A_g\bar{W}+B\bar{K}_g & 0 \\ \hline (*) & (2,2) & (*) \\ 0 & \left[\frac{1}{2}(\bar{P}_h-\bar{P}_g)\right]_{h\in\mathbb{N}_s\setminus\{g\}} & \left[X_{gh}\right]^{\mathbf{d}}_{h\in\mathbb{N}_s\setminus\{g\}} \end{array}\right] \tag{41}$$

where

$$(2,2) = -2\mu\bar{P}_g + \alpha\bar{P}_g + \sum_{h\in\mathbb{N}_s\setminus\{g\}} \rho_{gh}(\bar{P}_h - \bar{P}_g) - \sum_{h\in\mathbb{N}_s\setminus\{g\}} \bar{\delta}_{gh}^2 X_{gh}.$$

Then, the closed-loop system (16) is stochastically stable, and the mode-dependent control gain is constructed as follows: $K_g = \bar{K}_g\bar{W}^{-1}$.

Proof. After eliminating conditions (36) and (37), along with the associated decision variables, the remainder of the proof proceeds in the same manner as that of Theorem 1. □

Remark 5. *The novelty of the proposed method lies in the development of a transition-rate-dependent local tracking control framework for Markovian jump systems. Unlike existing MJS-based controllers, which mainly focus on regulation or global stabilization, the proposed framework explicitly integrates tracking performance with local stabilization, which guarantees tracking within a prescribed operating region under stochastic load-resistance switching.*

Remark 6. *The proposed controller guarantees local stability within the DOA characterized by a positively invariant level set of the Lyapunov function. Since the DOA may vary with the operating*

mode, a bring-up control can be employed after a mode transition to drive the system state into the corresponding DOA. Once the state enters the DOA, the proposed controller guarantees local stability. Otherwise, the theoretical stability guarantee no longer applies.

4. Simulation Results

The parameters of the considered buck converter (6)–(8) are listed in Table 1. As shown in Table 1, the equilibrium point of $v_C(t)$ is given by $\bar{v}_C = 5$. In this paper, the load variation is modeled as four discrete resistance modes $R_g \in \{5\,\Omega, 10\,\Omega, 15\,\Omega, 20\,\Omega\}$ for $g = 1, \cdots, 4$, and the switching between these modes follows a Markovian jump process characterized by the transition-rate matrix satisfying

- center of the uncertainty: $\left[\rho_{gh}\right]_{g,h\in\mathbb{N}_4} = \begin{bmatrix} -3.8 & 1.4 & 1.2 & 1.2 \\ 1.3 & -3.6 & 1.1 & 1.2 \\ 1.2 & 1.2 & -3.8 & 1.4 \\ 1.2 & 1.4 & 1.2 & -3.8 \end{bmatrix}$
- wide uncertainty: $\left[\bar{\delta}_{gh}\right]_{g,h\in\mathbb{N}_4} = \begin{bmatrix} 1.5 & 0.5 & 0.5 & 0.5 \\ 0.5 & 1.5 & 0.5 & 0.5 \\ 0.5 & 0.5 & 1.5 & 0.5 \\ 0.5 & 0.5 & 0.5 & 1.5 \end{bmatrix}$.

Table 1. Parameters of the buck converter.

Parameters	Value
Nominal input voltage v_I	12 V
Equilibrium point of $v_C(t)$	5 V
Inductance L	47 µH
Capacitance C	220 µF
Static drain-to-source resistance R_{DS}	30 mΩ
Equivalent series resistance of inductor R_{DCR}	100 mΩ
Equivalent series resistance of capacitor R_{ESR}	105 mΩ
Load resistance R_g	5, 10, 15, 20 Ω
Switching frequency	150 kHz

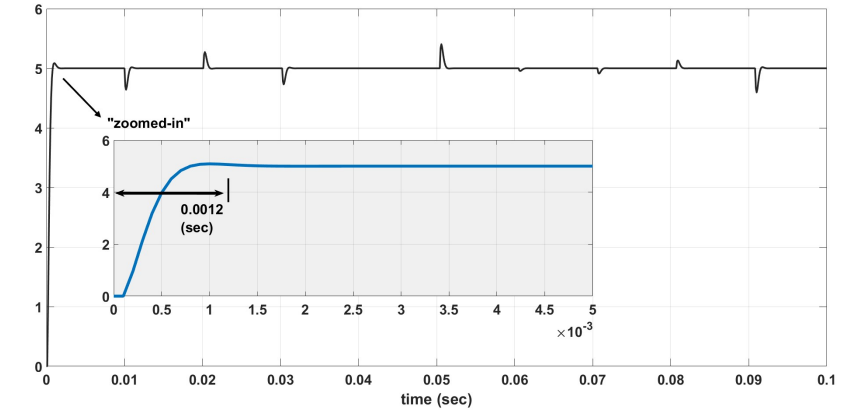
As a result, system (14) can be represented as follows:

$$A_1 = 10^3 \times \begin{bmatrix} -4.9541 & -20.839 \\ 4.4520 & -0.8904 \end{bmatrix}, \; A_2 = 10^3 \times \begin{bmatrix} -4.9768 & -21.056 \\ 4.4982 & -0.4498 \end{bmatrix}$$
$$A_3 = 10^3 \times \begin{bmatrix} -4.9845 & -21.129 \\ 4.5139 & -0.3009 \end{bmatrix}, \; A_4 = 10^3 \times \begin{bmatrix} -4.9883 & -21.165 \\ 4.5217 & -0.2261 \end{bmatrix}$$
$$B = 10^4 \times \begin{bmatrix} 2.1277 \\ 0 \end{bmatrix}.$$

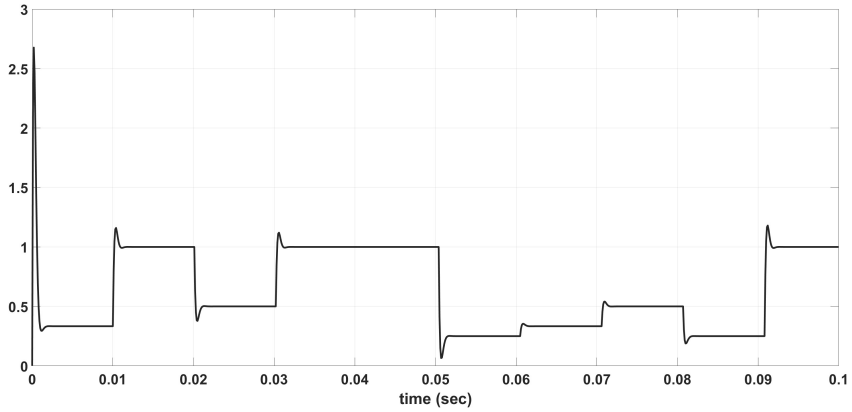
With the design parameters chosen as $\alpha = 0.5$, $\mu = 20$ and $\bar{x}_1 = \bar{x}_2 = 10^{-4}$, Theorem 1 yields the following solution for the above system model:

$$\bar{K}_1 = \begin{bmatrix} 0.0571 & 0.1492 \end{bmatrix}, \bar{K}_2 = \begin{bmatrix} 0.0564 & 0.1524 \end{bmatrix}$$
$$\bar{K}_3 = \begin{bmatrix} 0.0570 & 0.1535 \end{bmatrix}, \bar{K}_4 = \begin{bmatrix} 0.0550 & 0.1542 \end{bmatrix}$$
$$\bar{W} = \begin{bmatrix} 0.0560 & -0.1173 \\ 0.0774 & 0.1719 \end{bmatrix}.$$

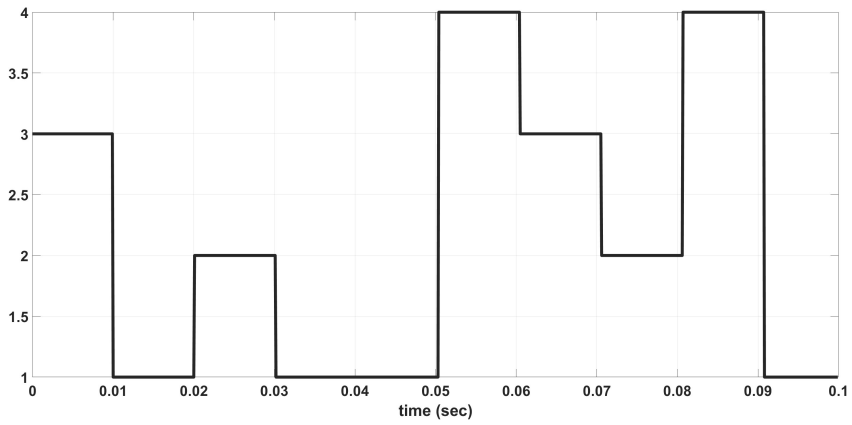
Figure 2 illustrates the time responses of the considered system under time-varying load conditions. Specifically, Figure 2a shows the capacitor voltage response $v_C(t)$, Figure 2b depicts the inductor current $i_L(t)$, and Figure 2c presents the load-side operating mode $\phi(t)$. As shown in Figure 2c, the load-side operating mode switches randomly among multiple discrete values, representing abrupt variations in the load condition. Despite these frequent and abrupt mode transitions, the capacitor voltage in Figure 2a remains well regulated around its desired reference value with only small transient deviations. The zoomed-in view further demonstrates that the voltage response exhibits a fast transient behavior, achieving regulation within approximately 0.0012 s, which indicates a rapid settling time. Meanwhile, Figure 2b shows that the inductor current $i_L(t)$ adjusts promptly in response to the load variations and operating mode changes. Although the current experiences step-like changes corresponding to the switching of $\phi(t)$, it remains bounded and does not exhibit excessive overshoot or oscillatory behavior. Figure 3 compares the system responses obtained under local stabilization (Theorem 1) and global stabilization (Corollary 1). Figure 3a illustrates the capacitor voltage response $v_C(t)$, while Figure 3b presents the corresponding inductor current $i_L(t)$. As shown in Figure 3a, both control designs successfully regulate the capacitor voltage to the desired operating level. However, a clear difference can be observed in their transient behaviors. Under the local stabilization framework (Theorem 1), the voltage response exhibits a fast and well-damped transient, reaching the steady-state region within approximately 0.014 s. In contrast, the global stabilization approach shows slower convergence and larger transient deviations, indicating inferior transient performance. Figure 3b further highlights the practical implications of this difference. When the local stabilization conditions of Theorem 1 are enforced, the inductor current exhibits a much smoother transient response with substantially reduced current peaks during abrupt load variations. In contrast, the global stabilization approach of Corollary 1 exhibits noticeable chattering and oscillatory current transients at each load-mode transition, resulting in significantly larger peak currents. Such excessive current excursions may increase electrical stress on power components and degrade overall system reliability. As summarized in Table 2, these results demonstrate that, although both approaches achieve voltage regulation, the proposed local stabilization strategy provides superior transient response. This comparison underscores the practical advantage of local stabilization when operating constraints and component protection are critical considerations. Moreover, Table 3 summarizes the feasibility of Theorem 1 for different combinations of the design parameters α and μ. It can be observed that the feasibility region gradually expands as μ increases. Accordingly, α should be selected to achieve the desired convergence performance while maintaining LMI feasibility, and μ can subsequently be adjusted to enlarge the feasible parameter region.



(**a**)



(**b**)

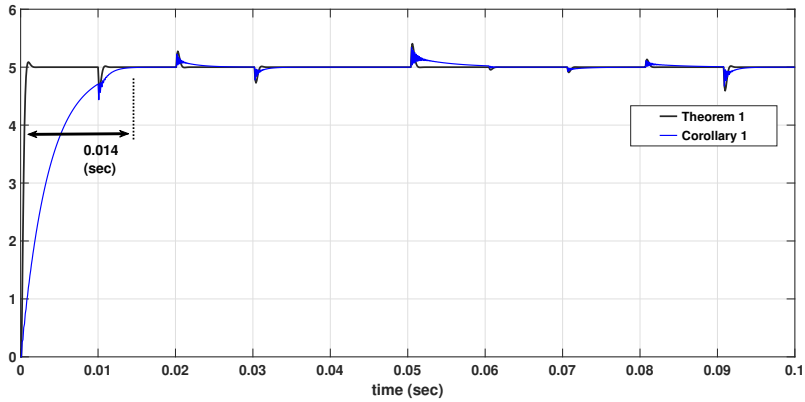


(**c**)

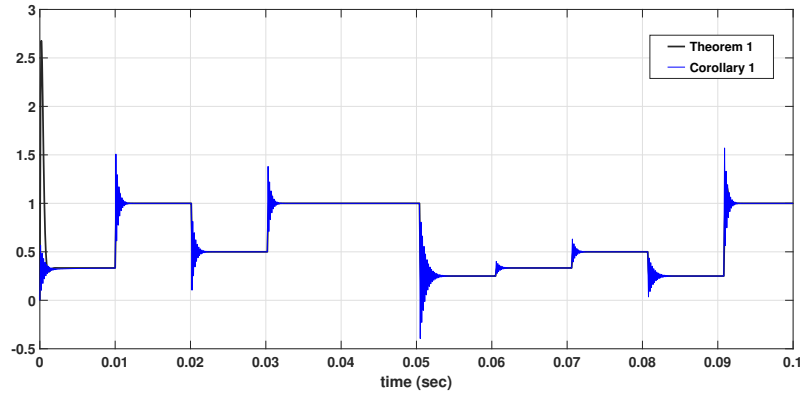
Figure 2. Time responses: (**a**) capacitor voltage $v_C(t)$. (**b**) Inductor current $i_L(t)$. (**c**) Load-side operating mode $\phi(t)$.

Table 2. Comparison of local and global tracking control performance.

Methods	Corollary 1	Theorem 1
settling time	0.014 s	0.0012 s
chattering phenomenon	absent	present



(**a**)



(**b**)

Figure 3. Comparison of system responses between local and global stabilization: (**a**) capacitor voltage $v_C(t)$. (**b**) Inductor current $i_L(t)$.

Table 3. Feasibility of Theorem 1 for α and μ (◯: feasible, ×: infeasible).

μ	$\alpha = 0.5$	5	10	20	40	60
10	◯	◯	◯	×	×	×
20	◯	◯	◯	◯	×	×
30	◯	◯	◯	◯	◯	×

Subsequently, Figure 4 illustrates the effect of the design parameter α on the transient responses of the proposed controller with the auxiliary parameter fixed at $\mu = 20$. As shown in Figure 4a, increasing α results in a faster rise in the capacitor voltage toward the desired reference. However, this improvement in convergence speed is accompanied by a larger voltage overshoot. In particular, the case of $\alpha = 20$ exhibits the fastest transient response but also the largest overshoot, whereas $\alpha = 0.5$ yields the slowest response with the smallest overshoot.

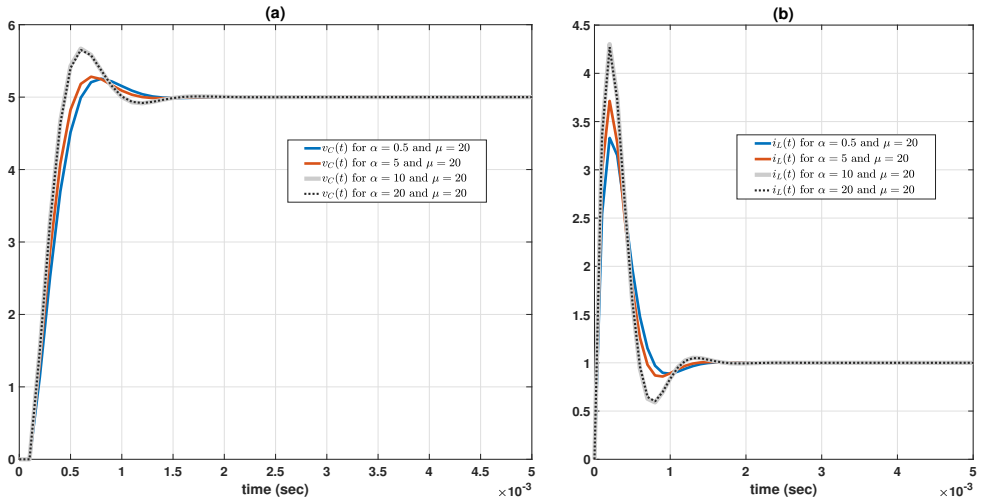


Figure 4. Time responses for different values of α: (**a**) Output voltage $v_C(t)$; (**b**) Inductor current $i_L(t)$.

Finally, to investigate the effect of transition-rate uncertainty on the domain of attraction, we additionally consider the following two transition-rate bound matrices:

- narrow uncertainty: $\left[\bar{\delta}_{gh}\right]_{g,h\in\mathbb{N}_4} = \begin{bmatrix} 0.3 & 0.1 & 0.1 & 0.1 \\ 0.1 & 0.3 & 0.1 & 0.1 \\ 0.1 & 0.1 & 0.3 & 0.1 \\ 0.1 & 0.1 & 0.1 & 0.3 \end{bmatrix}$
- no uncertainty: $\left[\bar{\delta}_{gh}\right]_{g,h\in\mathbb{N}_4} = \begin{bmatrix} 0.0 & 0.0 & 0.0 & 0.0 \\ 0.0 & 0.0 & 0.0 & 0.0 \\ 0.0 & 0.0 & 0.0 & 0.0 \\ 0.0 & 0.0 & 0.0 & 0.0 \end{bmatrix}$.

Figure 5 compares the estimated domains of attraction under different transition-rate uncertainty bounds. The case without transition-rate uncertainty yields the largest domain of attraction, whereas the domain gradually decreases as the uncertainty bound increases. This result is expected because a larger uncertainty bound requires the proposed LMI conditions to guarantee local stochastic stability over a broader set of admissible transition rates.

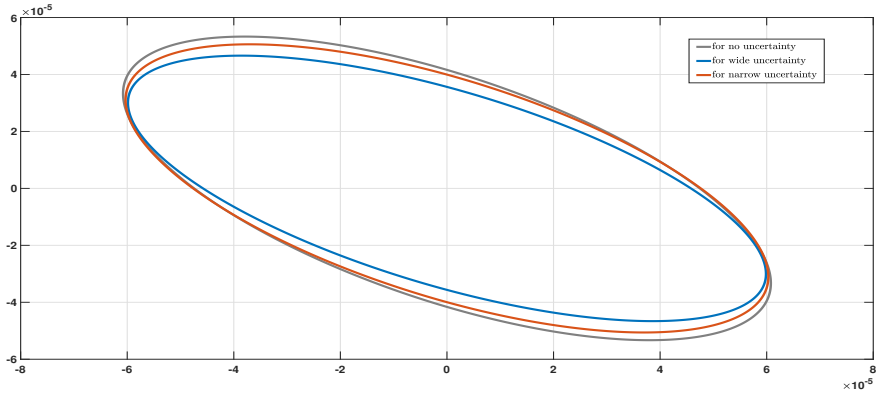


Figure 5. Estimated domains of attraction for different transition-rate uncertainty bounds.

Remark 7. *Our primary objective is to demonstrate that these additional constraints lead to improved closed-loop transient performance rather than to compare computational complexity or define dedicated performance metrics. Thus, although a quantitative comparison of com-*

putational complexity and dedicated performance metrics has not been provided, this paper demonstrates the effectiveness of the proposed local tracking method through its significantly improved transient performance.

Remark 8. *The primary objective of this paper is to demonstrate the effectiveness of the proposed transition-rate-dependent local tracking control framework. Accordingly, the proposed method is compared with the corresponding conventional global stabilization framework under the same system model, operating conditions, and controller structure, which provides a fair and consistent evaluation of the improvements achieved by the proposed local stabilization strategy.*

5. Concluding Remarks

This paper has presented a transition-rate-dependent local tracking control framework for DC–DC synchronous buck converters under stochastic load-resistance variations by modeling the converter as a Markovian jump system. The proposed mode-dependent state-feedback controller, together with the derived transition-rate-dependent LMI conditions, guarantees stochastic local stability and tracking performance within a prescribed domain of attraction while reducing the conservatism of conventional global-stabilization-based approaches. Simulation results have demonstrated that the proposed method achieves accurate voltage regulation, faster transient responses, and reduced peak inductor currents under randomly switching load conditions. Future research will extend the proposed framework to explicitly accommodate additional practical constraints, including inductance variations, capacitance aging, and switching delays.

Author Contributions: Conceptualization, S.H.K.; software, Y.J.C. and S.H.K.; validation, S.H.K.; writing—original draft, Y.J.C.; writing—review and editing, S.H.K.; visualization, Y.J.C.; supervision, S.H.K.; funding acquisition, S.H.K. All authors have read and agreed to the published version of the manuscript.

Funding: This work was supported by the 2026 Research Fund of University of Ulsan.

Data Availability Statement: The datasets presented in this article are not publicly available because they were generated as part of a government-funded research project, and their public release is restricted by the project agreement. We appreciate your understanding regarding this limitation.

Acknowledgments: This work was supported by the 2026 Research Fund of University of Ulsan.

Conflicts of Interest: The authors declare no conflicts of interest.

References

1. Abaali, H. Design modelling control and simulation of DC/DC power buck converter. *Int. J. Energy Power Eng.* **2015**, *9*, 1235–1299.
2. Hinov, N.; Kabakchieva, R.; Stanchev, P. A fuzzy satisfaction-based intelligent framework for multiobjective design of a buck DC-DC converter under uncertain operating conditions. *Mathematics* **2026**, *14*, 1115. [CrossRef]
3. Shi, L.F.; Jia, W.G. Mode-selectable high-efficiency low-quiescent-current synchronous buck DC–DC converter. *IEEE Trans. Ind. Electron.* **2013**, *61*, 2278–2285.
4. Jiang, D.; Fang, Y.; Fei, J. An extended-state observer based on smooth super-twisting sliding-mode controller for DC–DC buck converters. *Mathematics* **2023**, *11*, 2835. [CrossRef]
5. Lindiya, A.; Palani, S. Performance comparison of various controllers for DC–DC synchronous buck converter. *Procedia Eng.* **2012**, *38*, 2679–2693. [CrossRef]
6. Zahaf, A.; Bououden, S.; Chadli, M.; Boulkaibet, I.; Neji, B.; Khezami, N. Dynamic sensorless control approach for Markovian switching systems applied to PWM DC–DC converters with time-delay and partial input saturation. *Sensors* **2023**, *23*, 6936. [CrossRef] [PubMed]
7. Lee, W.; Shin, J.; Park, B. The strictly dissipative condition of continuous-time Markovian jump systems with uncertain transition rates. *Mathematics* **2024**, *12*, 639. [CrossRef]
8. Nguyen, T.B.; Song, H.K. Further results on robust output-feedback dissipative control of Markovian jump fuzzy systems with model uncertainties. *Mathematics* **2022**, *10*, 3620. [CrossRef]

9. Shi, P.; Li, F. A survey on Markovian jump systems: Modeling and design. *Int. J. Control Autom. Syst.* **2015**, *13*, 1–16. [CrossRef]
10. Zhao, P.; Kang, Y.; Zhao, Y.B. A brief tutorial and survey on Markovian jump systems: Stability and control. *IEEE Syst. Man Cybern. Mag.* **2019**, *5*, 37–43. [CrossRef]
11. Guo, Y.; Wang, Z. Stability of Markovian jump systems with generally uncertain transition rates. *J. Frankl. Inst.* **2013**, *350*, 2826–2836. [CrossRef]
12. Kao, Y.; Xie, J.; Wang, C. Stabilization of singular Markovian jump systems with generally uncertain transition rates. *IEEE Trans. Autom. Control* **2014**, *59*, 2604–2610. [CrossRef]
13. Yang, D.; Zhao, J.; Zong, G. Output regulation for switched LPV systems with Markovian jump parameters and its application. *Trans. Inst. Meas. Control* **2018**, *40*, 2831–2842. [CrossRef]
14. Boukas, E.K. $\mathcal{H}_\infty$ control of discrete-time Markov jump systems with bounded transition probabilities. *Optim. Control Appl. Methods* **2009**, *30*, 477–494. [CrossRef]
15. Hong, G.B.; Kim, S.H. Resilient adaptive event-triggered control of nonlinear DC-microgrids under DoS attacks: Local stabilization approach. *IEEE Trans. Autom. Sci. Eng.* **2025**, *22*, 11356–11368. [CrossRef]
16. Xu, N.; Yue, S.; Zhao, N.; Niu, B.; Zhao, X. SMS-Based optimal control of completely unknown nonlinear systems with unknown actuator saturation. *Int. J. Adapt. Control Signal Process.* **2026**, 1–16. [CrossRef]
17. de Souza, C.E.; Coutinho, D. Local stabilization of Markov jump nonlinear quadratic systems. In Proceedings of the IFAC Proceedings Volumes, Cape Town, South Africa, 24–29 August 2014; Volume 47, pp. 8725–8730.
18. Nguyen, N.H.A.; Kim, S.H. Relaxed robust stabilization conditions for nonhomogeneous Markovian jump systems with actuator saturation and general switching policies. *Int. J. Control. Autom. Syst.* **2019**, *17*, 586–596. [CrossRef]
19. Ding, Y.; Liu, H. Stability analysis of continuous-time Markovian jump time-delay systems with time-varying transition rates. *J. Frankl. Inst.* **2016**, *353*, 2418–2430. [CrossRef]
20. Li, Z.; Xu, Y.; Fei, Z.; Huang, H.; Misra, S. Stability analysis and stabilization of Markovian jump systems with time-varying delay and uncertain transition information. *Int. J. Robust Nonlinear Control* **2018**, *28*, 68–85. [CrossRef]
21. Zhao, J.; Xu, N.; Niu, B.; Alharbi, K.H.; Zhao, X. Fixed-time self-triggered adaptive neural practically tracking control for nonlinear systems with predefined output constraints. *Int. J. Robust Nonlinear Control* **2026**, 1–15. [CrossRef]
22. Nguyen, T.B.; Kim, S.H. Robust local stabilization of nonhomogenous Markovian jump fuzzy system with incomplete transition probabilities. In Proceedings of the 2019 7th International Conference on Control, Mechatronics and Automation (ICCMA), Delft, The Netherlands, 6–8 November 2019; pp. 21–25.
23. Babazadeh, A.; Corradini, L.; Maksimovic, D. Near time-optimal transient response in DC–DC buck converters taking into account the inductor current limit. In Proceedings of the 2009 IEEE Energy Conversion Congress and Exposition (ECCE), San Jose, CA, USA, 20–24 September 2009; pp. 3328–3335.
24. Zhao, S.; Liu, F. Bayesian estimation for jump Markov linear systems with non-homogeneous transition probabilities. *J. Frankl. Inst.* **2013**, *350*, 3029–3044. [CrossRef]
25. Mahdavi, J.; Emadi, A.; Toliyat, H.A. Application of state space averaging method to sliding mode control of PWM DC/DC converters. In Proceedings of the 1997 IEEE Industry Applications Conference (IAS'97), New Orleans, LA, USA, 5–9 October 1997; Volume 2, pp. 820–827.
26. Nguyen, N.H.A.; Kim, S.H. Asynchronous dissipative control design for semi-Markovian jump systems with uncertain probability distribution functions of sojourn-time. *Appl. Math. Comput.* **2021**, *397*, 125921. [CrossRef]
27. Wang, G.; Gao, X.; Li, X. Stabilization of Markovian jump systems via a partially mode-dependent controller of dwell times. *IEEE Access* **2019**, *7*, 161112–161122. [CrossRef]

Disclaimer/Publisher's Note: The statements, opinions and data contained in all publications are solely those of the individual author(s) and contributor(s) and not of MDPI and/or the editor(s). MDPI and/or the editor(s) disclaim responsibility for any injury to people or property resulting from any ideas, methods, instructions or products referred to in the content.